

Facile synthesized nanorod structured vanadium pentoxide for high-rate lithium batteries†

Anqiang Pan,^{ab} Ji-Guang Zhang,^{*b} Zimin Nie,^b Guozhong Cao,^c Bruce W. Arey,^b Guosheng Li,^b Shu-quan Liang^{*a} and Jun Liu^{*b}

Received 3rd May 2010, Accepted 19th July 2010

DOI: 10.1039/c0jm01306d

Nano-structured vanadium oxide (V_2O_5) is fabricated *via* a facile thermal-decomposition of vanadium precursor, vanadyl oxalate, which is produced by reacting micro-sized V_2O_5 with oxalic acid. The V_2O_5 nanoparticles produced by this method exhibit much better electrochemical performance than commercial micro-sized V_2O_5 . The optimized-nanorod electrodes give the best specific discharge capacities of 270 mAh g^{-1} at C/2 (147 mA g^{-1}) coupled with good cycle stability with only 0.32% fading per cycle. Even at a high rate of 4C (1176 mA g^{-1}), the nanorod electrode still delivers 198 mAh g^{-1} . These results suggest that the well-separated V_2O_5 nanorod is a good cathode material for high-rate lithium battery applications.

1. Introduction

Lithium ion batteries have been widely used as power sources for portable electronics in the last three decades because of their high energy density, long cycle life, and environmentally benign features.^{1–3} The state-of-the-art LiCoO₂ cathode used in many portable electronic devices has a specific capacity of ~140 mAh g^{-1} . Other new materials, such as LiFePO₄, have a capacity of up to 170 mAh g^{-1} and a high discharge rate. With increasing demands for rechargeable lithium ion batteries, especially for large-scale and high-power applications, such as plug-in hybrid electrical vehicles, alternative cost-effective cathode materials with high energy density have been extensively investigated. Vanadium pentoxide, due to its high energy density (the theoretical capacity of which reaches 440 mAh g^{-1} when three lithium ions are intercalated) and low cost, is considered to be a good candidate as a cathode for Li batteries.^{4–6} However, the intrinsic low-diffusion coefficient of lithium ions ($D \sim 10^{-12}$ cm² s⁻¹)⁷ and poor electronic conductivity (10^{-2} to 10^{-3} S cm⁻¹)⁸ in crystalline vanadium oxide (V_2O_5) hinder the practical application of this material. To improve the electrochemical performance, the utilization rate of the active material needs to be improved so that high discharge capacity and energy density can be delivered. Nanostructured materials provide a new opportunity to solve the problem by shortening the lithium ions' diffusion distance as a result of the reduced dimension of the particles. Electron transportation can be improved by making vanadium pentoxide-conductive composites.⁹ This strategy allows a low conductivity material to have good rate performance for large-scale applications. Various nanostructures of vanadium pentoxide, such as nanotubes, nanowires, nanofibers, nanobelts, nanorods, nanoflowers, and mesoporous

structures^{6,9–15} have been synthesized by different methods, including reverse-micelle synthesis, sol-gel and hydrothermal methods, and electrochemical deposition. Takahashi *et al.*¹⁶ synthesized single-crystal V_2O_5 nanorod arrays using template-based electrodeposition and the electrochemical results demonstrate that nanorod array electrodes have significantly higher current density and energy storage density than sol-gel-derived V_2O_5 films. However, it is difficult for large scale production and the removal of the template is still a challenge. Mohan *et al.*¹⁷ fabricated V_2O_5 nanotubes as cathode material for lithium battery by hydrothermal method using 1-hexadecylamine (HDA) and PEO as a template, the process is really time consuming (more than one week). These studies confirmed that nanostructured V_2O_5 delivered better electrochemical capabilities than bulk materials. However, most studies from the literature only obtained a high initial discharge capacity at a low discharge rate (usually less than 50 mA g^{-1}). Although vanadium pentoxide aerogels fabricated with the supercritical drying method possess good lithium ion intercalation at a high discharge rate, capacity retention still remains a question.^{18,19} In addition, reports for V_2O_5 electrode possessing high power performance as well as good cycle stability are rare. Therefore, fabricating electrodes with high discharge/charge capacity and good stability at a high rate is of great interest to the scientific community. Furthermore, low-cost and simple fabrication is important for practical applications.

In this paper, we report a cost-effective and template free method to synthesize nano-sized particles by thermal decomposition of vanadium precursors which are fabricated by using different molar ratios of micro-sized $V_2O_5/H_2C_2O_4$ (1 : 3 and 1 : 5). Thus-fabricated electrode exhibits high-rate discharge capacity and good cycle stability, which is among the best performance of V_2O_5 electrode ever reported. The correlation between the electrode performance and the electrode microstructures/morphologies will also be discussed.

2. Experimental section

Vanadium oxide (99.6%, Alfa Aesar), oxalic acid (99%, Aldrich), polyvinylidene fluoride (PVDF, Arkema Inc), 1-Methyl-2-pyrrolidinone

^aDepartment of Materials Science & Engineering, Central South University, Changsha, 410083, China. E-mail: lsq@mail.csu.edu.cn

^bPacific Northwest National Laboratory Richland, Washington, 99352, USA. E-mail: jun.liu@pnl.gov; jiguang.zhang@pnl.gov

^cDepartment of Materials Science & Engineering, University of Washington, Seattle, 98195, Washington, USA

† Electronic supplementary information (ESI) available: Further experimental results. See DOI: 10.1039/c0jm01306d

(NMP, Alfa Aesar), LiPF₆ (battery grade, Novolyte Technologies Inc.), ethylene carbonate (EC, battery grade, Novolyte Technologies Inc.) and dimethyl carbonate (DMC, battery grade, Novolyte Technologies Inc.) were used as-received without further purification. As purchased, micro-size V₂O₅ (1.2 g, 0.22 M) and H₂C₂O₄ (1.83 g, 0.67 M) in a stoichiometric ratio of 1 : 3 were added to 30 mL distilled water under active stirring (500 RMP) at room temperature until the color of the solution changed from yellow to blue. The solution was dried at 80 °C to produce the precursor and it was then calcined at 400 °C in air for 2 h. Another sample was prepared under similar conditions with a molar ratio of micro-size V₂O₅/H₂C₂O₄ = 1 : 5.

The crystalline structures of materials were determined by X-ray diffraction (XRD) using a Scintag XDS2000 θ - θ powder diffractometer equipped with a Ge(Li) solid-state detector and a Cu-K α sealed tube ($\lambda = 1.54178 \text{ \AA}$). All samples were scanned in a range between 10 and 70° (2θ), with a step size of 0.02° and an exposure time of 10 s. A scanning electron microscope (SEM) (FEI Helios 600 Nanolab FIB-SEM, 3 KV) was used to investigate the particle morphology. High-resolution transmission electron microscopy (TEM) analysis was carried out on a Jeol JEM 2100 microscope fitted with a LaB₆ filament and an acceleration voltage of 200 kV. A combined differential scanning calorimetry/TGA instrument (Netzsch, STA 449C) was used to study the decomposition and reaction of the precursors.

The electrochemical properties of the V₂O₅ nanoparticle and commercial V₂O₅ cathodes were tested in coin-cells with metallic lithium as the anode. For nanoparticles fabricated with a molar ratio of 1 : 3 of the starting reagents, the electrodes were made with the following different carbon content: a mixture containing active material/super P/PVDF = 8 : 1 : 1 and 7 : 2 : 1. For nanoparticles fabricated with a molar ratio 1 : 5 of the starting reagents, the mixture of the electrode was composed of active material/super P/PVDF = 7 : 2 : 1. The electrolyte was 1 M LiPF₆ in EC/DMC = 1 : 1 (volume ratio). Cyclic voltammetry (CV) measurements were performed using CHI 660C (CH Instrument Electrochemical workstation), and the discharge/charge measurements were performed on an Arbin BT-2000 battery tester at room temperature.

3. Results and discussion

3.1 Structural characterization

After commercial V₂O₅ powder was added to H₂C₂O₄ solution in a stoichiometric ratio of 1 : 3, the color of the liquid changed from yellow to blue, which indicated that the valence changed from V⁵⁺ to V⁴⁺, and the vanadium precursor, vanadyl oxalate hydrate (VOC₂O₄·nH₂O) was formed. The reaction can be expressed by eqn (1):²⁰



Fig. 1 shows the thermal gravimetric analysis (TG) and differential scanning calorimetry (DSC) results for the as-synthesized vanadyl oxalate (VOC₂O₄·nH₂O) precursor calcined in air. Three distinct stages were observed. The gradual weight loss from TG analysis and the endothermic peak in the first stage before 267 °C were attributed to the evaporation of the physically absorbed and chemically bonded water to vanadyl oxalate

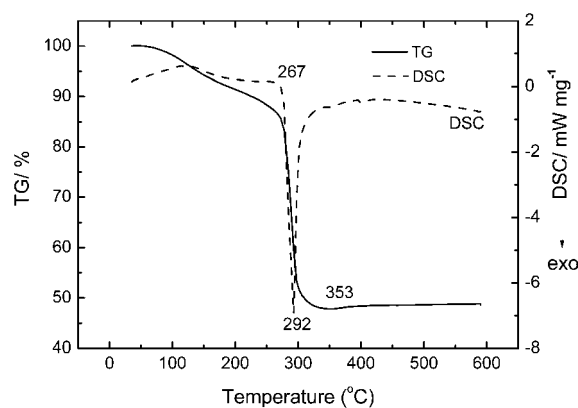


Fig. 1 TG pattern of vanadyl oxalate (VOC₂O₄·nH₂O) with molar ratio V₂O₅/H₂C₂O₄ = 1 : 3 in air; the heating rate was 5 °C min⁻¹, and heating flow rate was 50 mL min⁻¹.

(VOC₂O₄). Then a steep slope indicating a large weight loss and the exothermic peak of the DSC curve at 292 °C were observed, which demonstrated the successful thermal-decomposition of VOC₂O₄ to vanadium oxide. According to the mass loss, the production metal oxides were of mixed-valence (20% V⁴⁺ and 80% V⁵⁺) at 353 °C, and the slight increase of mass weight in the later stage after 353 °C was attributed to the further oxidation of VO₂ to V₂O₅.

The phase and purity of thermally decomposed sample and commercial V₂O₅ were determined by XRD, and the diffraction patterns are shown in Fig. 2. The XRD pattern of the calcined sample corresponds well to the commercial V₂O₅, and no other peaks were detected, indicating the high purity of as-synthesized V₂O₅. The peaks can be assigned to the orthogonal symmetry of V₂O₅ (space group: Pmmn, $a = 1.1516$, $b = 0.3566$, $c = 0.4372$ nm). However, the intensity of the peaks is much weaker and the breadth is wider, which suggests poor crystallinity and small crystallite particle size. According to the Scherrer method, crystallite dimensions of about 48 nm can be deduced from the (110) peak for the nanoparticles, which is much smaller than 60 nm for commercial V₂O₅.

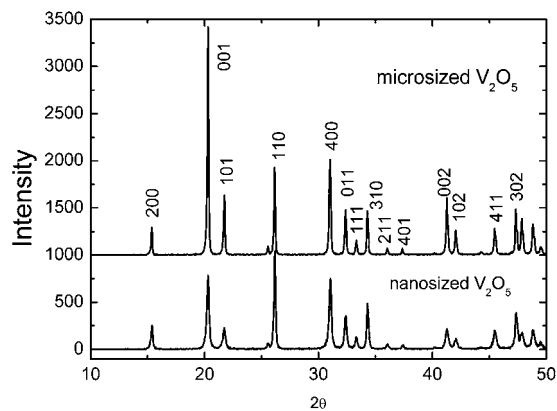


Fig. 2 XRD patterns of commercial V₂O₅ and nanosized V₂O₅ particles which were obtained from VOC₂O₄ precursor. The starting molar ratio of micro-sized V₂O₅ to H₂C₂O₄ is 1 : 3.

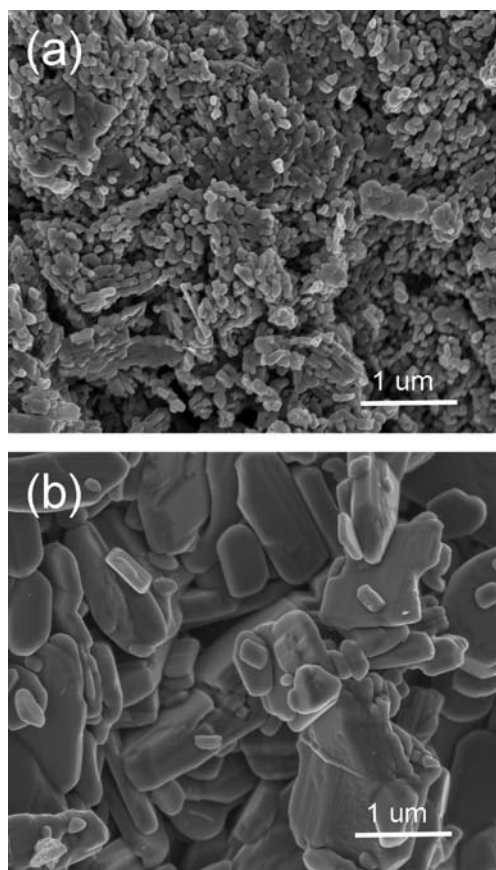


Fig. 3 SEM images of V_2O_5 particles: (a) nanoparticles synthesized by thermal decomposition at 400 °C for 2 h; (b) commercial micro-sized vanadium pentoxide.

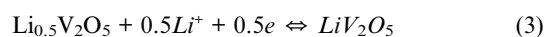
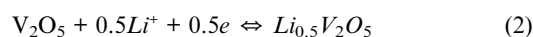
Fig. 3 shows the morphologies of the nanoparticles obtained by calcinating the precursor from a molar ratio 1 : 3 of starting reagents at 400 °C for 2 h (nominated as 13- V_2O_5 , see Fig. 3a) and commercial vanadium pentoxide (see Fig. 3b). As shown in Fig. 3b, the particle size of commercial V_2O_5 is around 1 μm , and its thickness is about 0.5 μm . For the thermally decomposed 13- V_2O_5 nanoparticles (see Fig. 3a), the particle size is much smaller than the starting V_2O_5 (Fig. 3b), and more voids are between particles. This was likely produced by the release of CO and CO_2 when the precursor decomposed during the calcination stage. The improved lithium ion intercalation properties in sample 13- V_2O_5 can be attributed to reduced particle dimensions as discussed later.

The surface morphologies of the products and structural information are shown in Fig. 4. Fig. 4a shows the SEM image of nanostructured V_2O_5 particles (13- V_2O_5), which were fabricated under thermal decomposition at 400 °C for 2 h with the molar ratio $V_2O_5/\text{H}_2\text{C}_2\text{O}_4 = 1 : 3$. The particles sizes range from 50 nm to 300 nm. The bigger particles might grow at the expense of the smaller ones to reduce the surface energy under a thermodynamic driving force when two particles merge at high temperature. To limit the aggregation of the final product, the oxalic acid content in the reagents was increased (molar ratio $V_2O_5/\text{H}_2\text{C}_2\text{O}_4 = 1 : 5$), which led to more uniform particles (nominated as 15- V_2O_5). The particles are much better separated with a void space between them (shown in Fig. 4b, 4c), and the particle size dispersion is

more uniform. Another finding is that the vanadium pentoxide nanoparticles have a rodlike morphology, and some neighboring particles are iso-oriented with each other. A close examination of the particle surface reveals small bumps and a rough surface of nanorod particles (Fig. 4c). The dimensions of the nanorods range from 20 nm to 100 nm. In the high-resolution TEM image of the nanorods (Fig. 4d, 4e), the surfaces of the crystals are covered by a thin layer of amorphous material, which corresponds to the bumps on the surface. The layer structures of vanadium pentoxide are also clearly observed in the HRTEM image. The typical layer distance is 0.43 nm. The V_2O_5 has a Pmmn structure with a lattice constant of $a = 1.15$ nm, $b = 0.356$ nm, and $c = 0.437$ nm.²¹ Along the c direction, the crystal is made of double layers of edge-sharing VO_5 square pyramids. The observed lattice planes are assigned to (001) planes since its layer distance of 0.43 nm agrees with the (001) plane distance. The FT-IR and Raman spectroscopy (shown in ESI†) of the nanorods are in good agreement with the V_2O_5 phase ever reported and demonstrate it is a single phase. The detailed discussion can be found in the ESI† and also, in which the effect of annealing temperature to the morphologies evolution of nanoparticles are revealed.

3.2 Electrochemical performance of nano-sized and micro-sized V_2O_5

Fig. 5 shows the CV curves of micro-sized V_2O_5 and nano-sized 13- V_2O_5 for lithiation-delithiation in the voltage range of 2 to 4 V vs. Li/Li^+ . As clearly shown in Fig. 5b, during a cathodic scan, three distinctive peaks were shown at 3.32, 3.12 and 2.17 V vs. Li/Li^+ , which indicated a multi-step lithium ion lithiation, and the corresponding phase was transformed from $\alpha\text{-}V_2O_5$ to $\varepsilon\text{-Li}_{0.5}V_2O_5$ (3.31 V), $\delta\text{-Li}V_2O_5$ (3.12 V), and $\gamma\text{-Li}_2V_2O_5$ (2.17 V), consecutively.^{22–24}



In the following anodic scan, three peaks were observed at 2.63, 3.35, and 3.49 V vs. Li/Li^+ . The first peak and the later two peaks were ascribed to the deintercalation of the second and first lithium ions.^{25–27} A CV experiment for commercially available micro-sized V_2O_5 was also carried out to compare the lithiation and delithiation process in the same voltage range. For its anodic scan, only two broad peaks were observed around 2.84 and 3.75 V vs. Li/Li^+ , which corresponded to the delithiation process. Comparing the two curves of different samples, it is apparent that the nano-sized V_2O_5 has less polarization, which was attributed to the reduced particle size. Another distinguishing feature is that the peak current density of nano-sized vanadium pentoxide electrode was almost twice as large as that of micro-particles of V_2O_5 . It has been reported that if the charge transfer at the interface is fast enough and the rate-limiting step is the lithium diffusion in electrode, then the peak current is proportional to the contact area between the electrode and the

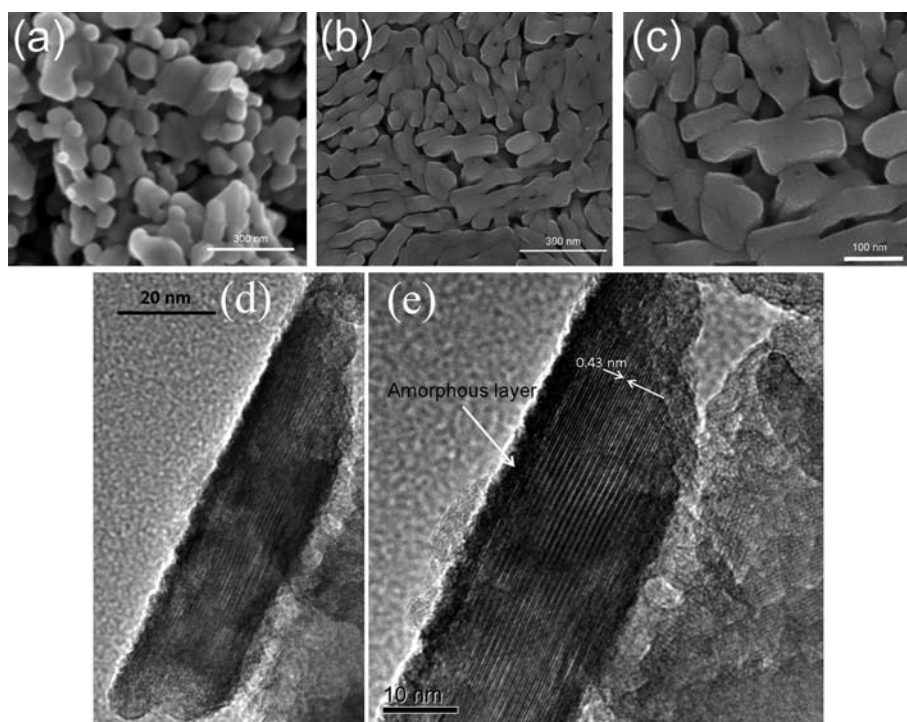


Fig. 4 Morphologies and structural information of 13- V_2O_5 and 15- V_2O_5 ; (a) SEM image of 13- V_2O_5 synthesized by thermal-decomposition of the precursor fabricated from the molar ratio of starting reagents $V_2O_5/H_2C_2O_4 = 1 : 3$ at 400 °C; (b, c) SEM images; (d, e) high-resolution transmission electron microscopy (HRTEM) images of 15- V_2O_5 nanoparticles from a precursor starting with molar ratio $V_2O_5/H_2C_2O_4 = 1 : 5$ at 400 °C.

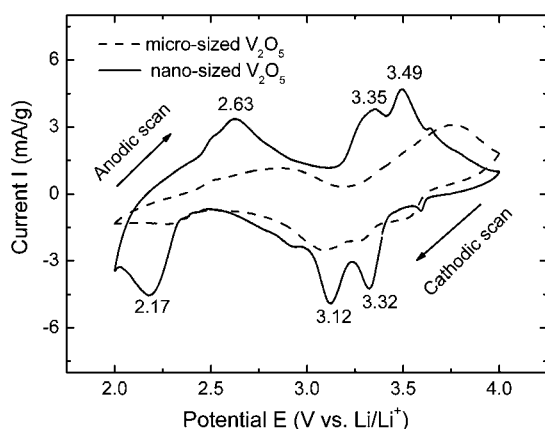


Fig. 5 CV curves of micro-sized (---) and nano-sized (—) vanadium pentoxide electrodes when cycled in a voltage range of 2 to 4 V vs. Li/Li^+ at a scan rate of 0.1 mVs^{-1} .

electrolyte.²⁸ In our case, the nanostructured vanadium pentoxide will certainly increase the contact surface area between electrode material and electrolyte, leading to a higher activity.

The discharge curves for the nano-sized vanadium pentoxide particles and the variation of discharge capacity *versus* cycle number plots are shown in Fig. 6. Three discharge plateaus, in agreement with the CV test results (Fig. 5), are shown in the discharge curves of 13- V_2O_5 nanoelectrode (Fig. 6a). A specific discharge capacity of 274 $mAhg^{-1}$ for the initial discharge was obtained at a low discharge rate ($C/20$). The capacity is close to the theoretic capacity (294 $mAhg^{-1}$ for 2 Li^+ intercalation). Compared to that of the micro-sized V_2O_5 , the discharge

capacity of the nano-sized V_2O_5 is much higher (shown in Fig. 6b). The high specific discharge capacity indicated a high utilization rate of V_2O_5 nanoparticles, which was derived from a high interfacial contact area between electrode and electrolyte and a shortened lithium ion diffusion and electron transportation distance. However, it should be mentioned that micro-sized V_2O_5 shows better cycle stability. This result is not surprising and is related to the limited lithium ion intercalation for the second lithium ion at 2.29 V vs. Li/Li^+ for micro-sized one (Fig. 5). It was reported²⁴ that the γ - $Li_2V_2O_5$ phase transition related to the second lithium ion is not as reversible as the ϵ - $Li_{0.5}V_2O_5$ and δ - LiV_2O_5 phase transition for the first lithium ion intercalation/deintercalation according to eqn (2) and 3. The multi-step transformation may destroy the crystal structure of V_2O_5 nanoparticles and increase cell resistance.

3.3 Rate performance improvement of V_2O_5 nanoparticle electrodes

For high-rate cathode usage, the electrons produced at the interface between electrode and electrolyte should be transferred immediately so that the reactions can happen rapidly. Although the nanoparticle electrode (13- V_2O_5) composed of 80% active materials ($(V_2O_5)/super\ P/binder\ (PVDF) = 8 : 1 : 1$) has a high discharge capacity at a low discharge rate ($C/20$), the discharge capacity at $C/2$ (147 mAg^{-1}) was not quite satisfactory (shown in Fig. 7). This phenomenon was explained by the poor conductivity of the electrode. The electron produced by the Faraday reaction can be sufficiently transferred at a low discharge rate. However, when operated under high current density, the intrinsic

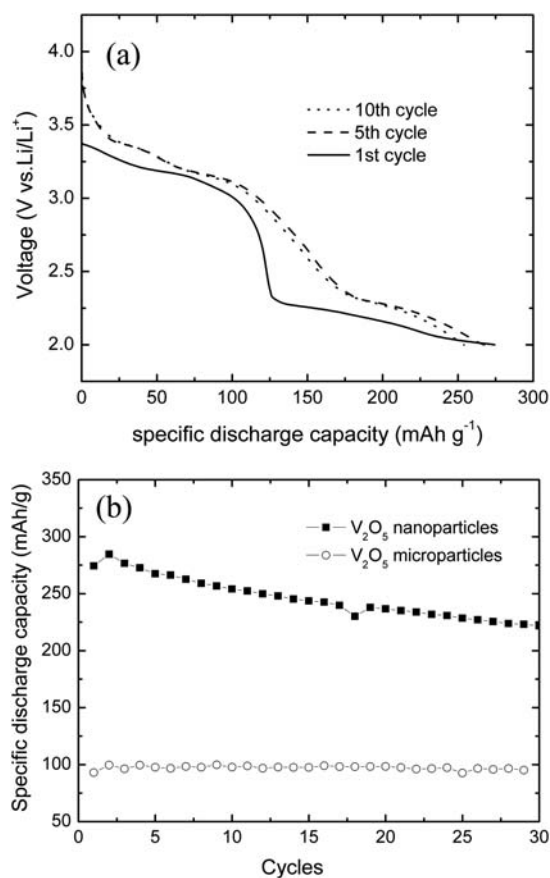


Fig. 6 (a) Discharge curves of the cell with V₂O₅ nanoparticles and (b) variation of discharge capacity *vs.* number of cycle plots of 13-V₂O₅ and micro-sized V₂O₅.

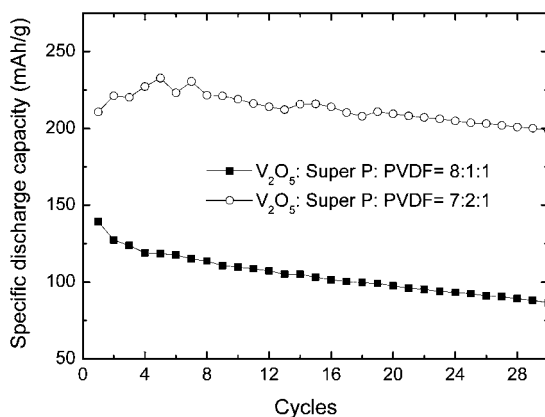


Fig. 7 Variation of discharge capacity *vs.* number of cycles for the lithium-ion batteries with different electrode composition (V₂O₅ : super P : PVDF = 8 : 1 : 1 and 7 : 2 : 1, respectively); the starting-materials have a molar ratio of V₂O₅/H₂C₂O₄ = 1 : 3, and the discharge rate was 147 mA g⁻¹.

low conductivity of vanadium pentoxide⁸ is still not good enough. To increase the electronic conductivity of the electrode, the content of conductive carbon, super P, was increased from 10% to 20% in the electrode during the slurry preparation process. Fig. 7 shows the electrochemical performances of the

electrodes with different carbon contents. A specific discharge capacity of 239 mA h g⁻¹ was observed for a higher carbon content (20%), which is doubled compared to 120 mA h g⁻¹ for a low-carbon-content (10%) electrode. Furthermore, the electrode with more carbon content exhibits better cycle stability. This is consistent with results reported in the literature that by increasing carbon in vanadium oxides and carbon composites, better electrochemical performance can be achieved^{27,29–35} because carbon served as a good current collector and fast-electron transportation medium.

As discussed earlier (see Fig. 3a and Fig. 4a), nano-sized V₂O₅ was successfully fabricated. However, some aggregation was detected, which led to particles coarsening. To effectively control aggregation, more oxalic acid was used to make the precursor and produce more homogenous V₂O₅ nanoparticles (as shown in Fig. 4b and 4c). Fig. 8 shows the discharge curve and the specific discharge capacity *versus* cycle-number plots of nanoparticle electrodes calcined from different molar ratios of starting reagents (1 : 3 and 1 : 5) at 400 °C. The fifth cycle discharge curves for 13-V₂O₅ and 15-V₂O₅ nanoparticle electrodes with the same carbon content (20%) are shown in Fig. 8a. Three plateaus corresponding to lithium ion intercalation to the host materials were clearly observed for both electrodes, which demonstrated the phase transition from α-V₂O₅ to ε-Li_{0.5}V₂O₅, δ-LiV₂O₅, and γ-Li₂V₂O₅ at C/2. As shown in Fig. 8a, the 15-V₂O₅ electrode with more oxalic acid gave a higher specific discharge capacity of

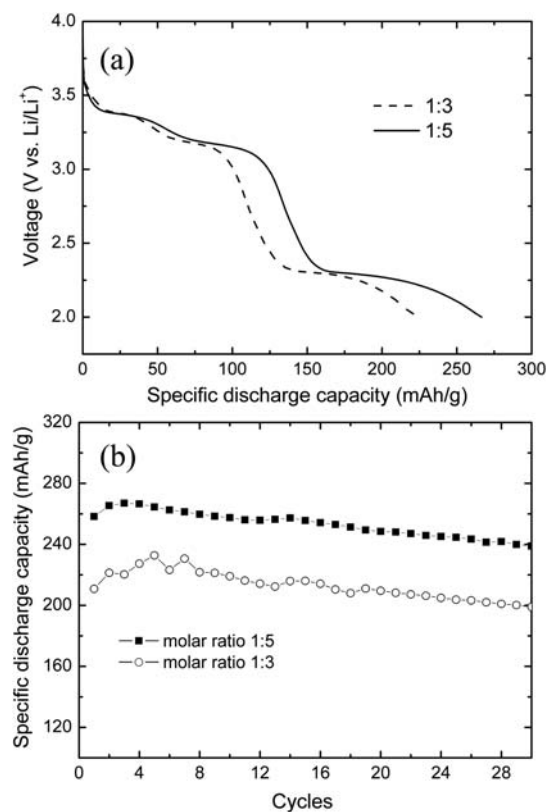


Fig. 8 (a) Discharge curves of the fifth cycle and (b) variation of discharge capacity *versus* numbers of the cell of as-synthesized nanoparticles 13-V₂O₅ and 15-V₂O₅. The electrode was composed of 70% active material, 20% super P, and 10% PVDF.

266 mAh g⁻¹, more than the 239 mAh g⁻¹ for the 13-V₂O₅ electrode. After 30 cycles, the two samples still retained a specific discharge capacity of 240 mAhg⁻¹ and 198 mAhg⁻¹, respectively. These values were much higher than the flame spray-pyrolyzed nano-V₂O₅ electrode,²⁴ which only possessed a discharge capacity of 150 mAhg⁻¹ after 30 cycles. The cycle stability of both samples is shown in Fig. 8b, and the specific capacity fading rates between fifth and thirtieth cycles for 13-V₂O₅ and 15-V₂O₅ were 0.53% and 0.32% per cycle, respectively. The superior discharge capacity retention compared to the results of other nanostructured vanadium pentoxide electrodes reported in the literature may be attributed to the combined effect of high purity and as well as well-separated nanoparticles. It is believed that the well-separated crystallites and extra space between them allows the active material expand freely with lithium ions intercalation, which lowers the energy barrier for lithium ion diffusion to achieve high performances. This phenomenon was reported recently by Dunn and co-workers for iso-oriented MoO₃ crystallites effectively leading to intercalation pseudocapacitance.³⁵ The higher specific discharge capacity and better stability of 15-V₂O₅ with respect to 13-V₂O₅ may be due to limited aggregation. From the SEM of 15-V₂O₅ (Fig. 4b, 4c), the nanoparticles were dispersed more homogeneously, and much more space was observed between each particle. Another interesting feature is that the shape of 15-V₂O₅ particles exhibited a nanorod-like structure, which was around 20 nm to 100 nm wide and well aligned to one direction at a local area. This alignment can support an easier path for electrolyte penetration. Furthermore, the amorphous surface of rodlike nanoparticles (Fig. 4e) related to the bumps on the surface of the particles would increase the interfacial contact area, which is associated with the high-discharge capacity. Also, much well-separated nanoparticles can accompany well with the phase transition and volume change. All these features would help increase the specific discharge capacity and the use of the active material at a high discharge rate.

Fig. 9 plots the specific discharge capacity *versus* cycle numbers of 15-V₂O₅ electrodes composed of 15-V₂O₅/super P/PVDF = 7 : 2 : 1 at a different discharge/charge rate. The specific discharge capacity at the C/2 (147 mA g⁻¹) rate could reach 270 mAhg⁻¹, close to the theoretical capacity (290 mAhg⁻¹) for two

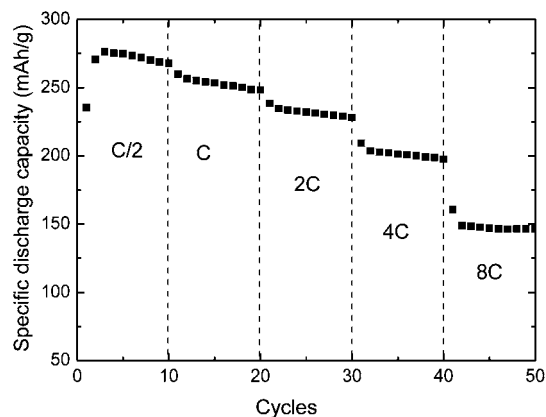


Fig. 9 The rate performance of a 15-V₂O₅ electrode from 2 to 4 V vs. Li/Li⁺ at the same discharge/charge rate for each cycle. Here 1C = 294 mA g⁻¹.

lithium ion intercalations. The value decreased to 256 mAhg⁻¹ at 1C (294 mA g⁻¹), 234 mAhg⁻¹ at 2C (588 mA g⁻¹), 198 mAhg⁻¹ at 4C (1176 mA g⁻¹), and 144 mAhg⁻¹ at 8C (2352 mA g⁻¹). This rate capability is much better compared to the results reported in the literature. For example, double-shelled nanocapsules of V₂O₅-based composites³⁶ gave a specific discharge capacity of 250 mAhg⁻¹ at 50 mA g⁻¹, 200 mAhg⁻¹ at 250 mA g⁻¹, and 160 mAhg⁻¹ at 500 mA g⁻¹. Our results are also better when compared to carbon-coated V₂O₅^{27,29} and possess a similar rate performance to a V₂O₅/carbon tube-in-tube composite,³⁷ but the synthesis of the V₂O₅/carbon tube-in-tube structure is much more complicated.

4. Conclusion

In summary, a facile synthesis method has been developed for preparing nano-sized vanadium pentoxide (V₂O₅) by thermal decomposition of vanadyl oxalate in air. These new materials have a much better electrochemical performance as compared to micro-sized V₂O₅. The rate performance of the nanoparticle electrodes is improved by increasing the carbon content when making the electrode. By increasing the molar ratio of oxalic acid in the starting reagents, a novel V₂O₅ with well-aligned rodlike nanoparticles was synthesized, and it exhibited excellent discharge capacity and cycle stability at high-rate discharge/charge processes. The good performance is attributed to the following facts: (1) shortened Li⁺-ion diffusion distance and well dispersion of the nanoparticles (2) a locally iso-oriented nanorod structure and void space between particles for electrolyte easy penetration, and (3) well-separated crystallites accompany well with the phase transition and lower the energy barrier for lithium ion diffusion. The nanostructured vanadium pentoxide prepared by this method produces good cathode Li batteries for high-power applications.

Acknowledgements

We acknowledge the support from the National Nature Science Foundation of China (No. 50774097), the Creative Research Group of the National Natural Science Foundation of China (No. 50721003), and the Laboratory Directed Research and Development Program of Pacific Northwest National Laboratory (PNNL). The TEM work was performed at the Environmental Molecular Sciences Laboratory, a national scientific-user facility sponsored by the U.S. Department of Energy's (DOE's) Office of Biological and Environmental Research and located at PNNL with support from DOE, Office of Basic Energy Sciences, Division of Materials Sciences and Engineering under Award KC020105-FWP12152. PNNL is operated by Battelle for DOE under Contract DE-AC05-76RL01830. We thank Drs. Deyu Wang, Jie Xiao and Wu Xu for their assistance in cell preparation and Dr Chongmin Wang for the discussion of TEM work.

References

- 1 J. M. Tarascon and M. Armand, *Nature*, 2001, **414**, 359–367.
- 2 J. Hassoun, P. Reale and B. Scrosati, *J. Mater. Chem.*, 2007, **17**, 3668–3677.
- 3 R. Koksang, J. Barker, H. Shi and M. Y. Saidi, *Solid State Ionics*, 1996, **84**, 1–21.

- 4 E. A. Ponzio, T. M. Benedetti and R. M. Torresi, *Electrochim. Acta*, 2007, **52**, 4419–4427.
- 5 Y. Wang, Cao and G. Z., *Adv. Mater.*, 2008, **20**, 2251–2269.
- 6 Y. Wang, K. Takahashi, K. Lee and G. Z. Cao, *Adv. Funct. Mater.*, 2006, **16**, 1133–1144.
- 7 T. Watanabe, Y. Ikeda, T. Ono, M. Hibino, M. Hosoda, K. Sakai and T. Kudo, *Solid State Ionics*, 2002, **151**, 313–320.
- 8 J. Muster, G. T. Kim, V. Krstic, J. G. Park, Y. W. Park, S. Roth and M. Burghard, *Adv. Mater.*, 2000, **12**, 420–424.
- 9 A. S. Arico, P. Bruce, B. Scrosati, J. M. Tarascon and W. Van Schalkwijk, *Nat. Mater.*, 2005, **4**, 366–377.
- 10 A. M. Cao, J. S. Hu, H. P. Liang and L. J. Wan, *Angew. Chem., Int. Ed.*, 2005, **44**, 4391–4395.
- 11 K. Takahashi, Y. Wang and G. Z. Cao, *Appl. Phys. Lett.*, 2005, **86**, 053102.
- 12 X. Chen, X. M. Sun and Y. D. Li, *Inorg. Chem.*, 2002, **41**, 4524–4530.
- 13 K. Takahashi, S. J. Limmer, Y. Wang and G. Z. Cao, *J. Phys. Chem. B*, 2004, **108**, 9795–9800.
- 14 K. Takahashi, S. J. Limmer, Y. Wang and G. Z. Cao, *Japanese Journal of Applied Physics Part 1-Regular Papers Brief Communications & Review Papers*, 2005, **44**, 662–668.
- 15 J. K. Lee, G. P. Kim, I. K. Song and S. H. Baeck, *Electrochem. Commun.*, 2009, **11**, 1571–1574.
- 16 K. Takahashi, S. J. Limmer, Y. Wang and G. Z. Cao, *J. Phys. Chem. B*, 2004, **108**, 9795–9800.
- 17 V. M. Mohan, B. Hu, W. L. Qiu and W. Chen, *J. Appl. Electrochem.*, 2009, **39**, 2001–2006.
- 18 M. J. Parent, S. Passerini, B. B. Owens and W. H. Smyrl, *J. Electrochem. Soc.*, 1999, **146**, 1346–1350.
- 19 S. Passerini, J. J. Ressler, D. B. Le, B. B. Owens and W. H. Smyrl, *Electrochim. Acta*, 1999, **44**, 2209–2217.
- 20 M. M. Ren, Z. Zhou, X. P. Gao, W. X. Peng and J. P. Wei, *J. Phys. Chem. C*, 2008, **112**, 5689–5693.
- 21 Galy, *J. Solid State Chem.*, 1992, **100**, 229–245.
- 22 R. J. Cava, A. Santoro, D. W. Murphy, S. M. Zahurak, R. M. Fleming, P. Marsh and R. S. Roth, *J. Solid State Chem.*, 1986, **65**, 63–71.
- 23 M. Broussely, F. Perton, J. Labat, R. J. Staniewicz and A. Romero, *J. Power Sources*, 1993, **43**, 209–216.
- 24 S. H. Ng, T. J. Patey, R. Buechel, F. Krumeich, J. Z. Wang, H. K. Liu and S. E., *Phys. Chem. Chem. Phys.*, 2009, **11**, 3748–3755.
- 25 M. Koltypin, V. Pol, A. Gedanken and D. Aurbach, *J. Electrochem. Soc.*, 2007, **154**, A605–A613.
- 26 J. S. Braithwaite, C. R. A. Catlow, J. D. Gale and J. H. Harding, *Chem. Mater.*, 1999, **11**, 1990–1998.
- 27 A. Odani, V. G. Pol, S. V. Pol, M. Koltypin, A. Gedanken and D. Aurbach, *Adv. Mater.*, 2006, **18**, 1431–1436.
- 28 X. H. Rui, N. Ding, J. Liu, C. Li and C. H. Chen, *Electrochim. Acta*, 2010, **55**, 2384–2390.
- 29 N. S. Ergang, J. C. Lytle, K. T. Lee, S. M. Oh, W. H. Smyrl and A. Stein, *Adv. Mater.*, 2006, **18**, 1750–1753.
- 30 W. C. Fang and W. L. Fang, *Chem. Commun.*, 2008, 5236–5238.
- 31 J. S. Sakamoto and B. Dunn, *J. Electrochem. Soc.*, 2002, **149**, A26–A30.
- 32 B. C. Satishkumar, A. Govindaraj, M. Nath and C. N. R. Rao, *J. Mater. Chem.*, 2000, **10**, 2115–2119.
- 33 A. Q. Pan, D. W. Liu, X. Y. Zhou, B. B. Garcia, S. Q. Liang, J. Liu and G. Z. Cao, *J. Power Sources*, 2010, **195**, 3893–3899.
- 34 Z. Chen, Y. C. Qin, D. Weng, Q. F. Xiao, Y. T. Peng, X. L. Wang, H. X. Li, F. Wei and Y. F. Lu, *Adv. Funct. Mater.*, 2009, **19**, 3420–3426.
- 35 T. Brezesinski, J. Wang, S. H. Tolbert and B. Dunn, *Nat. Mater.*, 2010, **9**, 146–151.
- 36 J. Liu, H. Xia, D. F. Xue and L. Lu, *J. Am. Chem. Soc.*, 2009, **131**, 12086–12087.
- 37 Y. S. Hu, X. Liu, J. O. Muller, R. Schlogl, J. Maier and D. S. Su, *Angew. Chem., Int. Ed.*, 2009, **48**, 210–214.